2015-01-0602
Published 04/14/2015

doi:10.4271/2015-01-0602
saematman.saejournals.org

Effects of Non-Associated Flow on Residual Stress Distributions in Crankshaft Sections Modeled as Pressure-Sensitive Materials under Fillet Rolling

Shin-Jang Sung and Jwo Pan
University of Michigan

Mohammed Yusuf Ali, Jagadish Sorab, and Cagri Sever
Ford Motor Company

ABSTRACT

In this paper, the evolution equation for the active yield surface during the unloading/reloading process based on the pressure-sensitive Drucker-Prager yield function and a recently developed anisotropic hardening rule with a non-associated flow rule is first presented. A user material subroutine based on the anisotropic hardening rule and the constitutive relation was written and implemented into the commercial finite element program ABAQUS. A two-dimensional plane strain finite element analysis of a crankshaft section under fillet rolling was conducted. After the release of the roller, the magnitude of the compressive residual hoop stress for the material with consideration of pressure sensitivity typically for cast irons is smaller than that without consideration of pressure sensitivity. In addition, the magnitude of the compressive residual hoop stress for the pressure-sensitive material with the non-associated flow rule is smaller than that with the associated flow rule. The computational results indicate that without consideration of pressure sensitivity and the non-associated flow rule, the residual stresses in crankshaft sections under fillet rolling are overestimated.

CITATION: Sung, S., Pan, J., Ali, M., Sorab, J. et al., "Effects of Non-Associated Flow on Residual Stress Distributions in Crankshaft Sections Modeled as Pressure-Sensitive Materials under Fillet Rolling," *SAE Int. J. Mater. Manf.* 8(2):2015, doi:10.4271/2015-01-0602.

INTRODUCTION

Crankshafts in automotive engines can experience a significant number of service cyclic loads. Since fatigue cracks initiated near the fillet can lead to one of the primary failure mechanisms of automotive crankshafts, fillet rolling processes have been used to improve the fatigue lives of crankshafts for many years. Based on the results of the recent research works [1, 2, 3, 4, 5], accurate predictions of the distributions of residual stresses up to a few millimeters from the fillet surface are very important to determine the fatigue failure process and the fatigue limit of crankshaft sections.

Cast irons are commonly used for gasoline engine crankshafts for good mechanical property and, above all, the ability to be cast into complex shape at low cost. It is well known that the tensile and compressive yield behaviors of cast irons are different due to the existence of graphite particles. The different yield behaviors under tension and compression can be modeled by a pressure-sensitive yield function. The material elements near the fillets under rolling are usually subjected to cyclic loading/unloading conditions. Current commercial finite element codes cannot be used to model the materials with the different tensile and compressive yield behaviors under cyclic loading conditions as discussed in Choi and Pan [4].

The yield functions to describe pressure-sensitive yielding behavior usually involve the hydrostatic stress and the second invariant of the deviatoric stress [6, 7, 8, 9]. However, with the associated flow rule, the pressure-sensitive yield functions usually lead to a plastic dilatancy which is at least an order of magnitude larger than that observed in experiments [8,9]. Therefore, non-associated flow rules based on pressure-sensitive yield functions were adopted to properly model the plastic behaviors of pressure-sensitive materials under monotonic loading conditions [10, 11, 12].

Recently, Choi [13] formulated a generalized anisotropic hardening rule based on a general yield function to model cyclic plastic behavior of materials based on the concepts of the Mroz model [14,15]. The closed-form solutions for one-dimensional stress-plastic strain curves were also derived and plotted for materials under cyclic loading conditions based on the Mises yield function, the Hill quadratic anisotropic yield function and the Drucker-Prager yield function. For materials based on the Drucker-Prager yield function with the associated flow rule, the stress-plastic strain curves do not close and show an unusually large ratcheting effects under uniaxial cyclic loading conditions. The unusually large ratcheting effect contradicts the nearly closed hysteresis loops of cast irons under cyclic loading conditions observed in experiments. Therefore, Choi [13] proposed an anisotropic hardening rule with a conventional and a non-conventional non-associated flow rules in order to take away the large ratcheting effects. The anisotropic hardening rule of Choi [13] with the conventional non-associated flow rule is adopted here to characterize the pressure-sensitive cyclic plastic behavior of the cast

iron crankshaft section during the fillet rolling process since the current commercial finite element codes do not provide a cyclic plasticity model for pressure-sensitive materials such as cast irons.

Choi and Pan [5] adopted the anisotropic hardening rule of Choi [13] based on the Drucker-Prager function with the non-conventional non-associated flow rule to investigate the stress distributions near the fillet of a crankshaft section under fillet rolling and subsequent bending. Their constitutive relation based on the tangent modulus procedure for rate-sensitive materials was formulated and implemented into a user material subroutine for ABAQUS. A two-dimensional plane-strain finite element analysis of a crankshaft section under fillet rolling and subsequent bending was conducted for different values of the pressure sensitivity in order to investigate the effect of the pressure-sensitive yielding and the non-conventional non-associated flow rule on the stress distributions near the fillet. The computational results showed that, as the pressure sensitivity increases, the maximum tensile stress at the fillet surface increases and the size of the tensile stress region increases after the release of roller and under subsequent bending.

In this paper, the evolution equation for the active yield surface during the unloading/reloading process based on the anisotropic hardening rule of Choi [13] and the Drucker-Prager yield function is first presented. A user material subroutine based on the anisotropic hardening rule and the constitutive relation for rate-insensitive materials was written and implemented into the commercial finite element program ABAQUS. A two-dimensional plane strain finite element analysis of a crankshaft section under fillet rolling was conducted for different values of the pressure sensitivity and different flow rules in order to investigate the effect of the pressure-sensitive yielding and the non-associated flow rule on the stress distributions near the fillet. The residual stress distributions after the release of the roller are obtained and compared for pressure-insensitive and pressure-sensitive materials with both the associated and the conventional non-associated flow rule. Finally, some conclusions based on the computational results are made.

AN ANISOTROPIC HARDENING RULE OF CHOI [13]

Choi [13] developed a cyclic plasticity theory for materials based on a general yield function. Fig. 1 shows the evolution of the active yield surface during the unloading/reloading process based on the anisotropic hardening rule of Choi [13]. As shown in Fig. 1, the active yield surface $\mathbf{\Phi}_A$ continuously expands with the unloading stress point $\sigma_{ij}^{M,t}$ being kept as the tangential contact point and the center α_{ij}^A also continuously moves along the line joining the unloading stress point $\sigma_{ij}^{M,t}$ to the center α_{ij}^M of the largest yield surface previously reached. The yield surface $\mathbf{\Phi}_M$ is a memory yield surface which is used to determine the subsequent plastic behavior during the unloading/reloading process. The unloading stress point $\sigma_{ij}^{M,t}$ is defined whenever the unloading takes place.

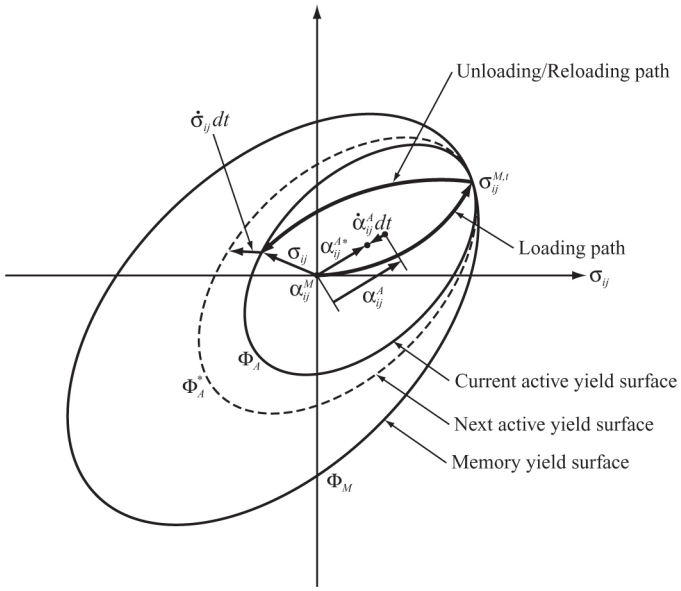

Figure 1. A schematic plot of the evolution of the active yield surface during the unloading/reloading process based on the anisotropic hardening rule of Choi [13].

In Fig. 1, the similarity condition for the memory yield surface and the active yield surface can be expressed as

$$\frac{\sigma_{ij}^{M,t}-\alpha_{ij}^{M}}{\bar{\sigma}_M}=\frac{\sigma_{ij}^{M,t}-\alpha_{ij}^{A}}{\bar{\sigma}_A} \tag{1}$$

where $\bar{\sigma}_M$ and $\bar{\sigma}_A$ represent the sizes of the memory yield surface and the active yield surface, respectively, and α_{ij}^M and α_{ij}^A represent the centers of these yield surfaces, respectively. The evolution equation for α_{ij}^A along the line joining the centers of the active yield surface and the memory yield surface can be obtained from the differentiation of Eq. (1) as

$$\dot{\alpha}_{ij}^{A}=-\left(\frac{\sigma_{ij}^{M,t}-\alpha_{ij}^{M}}{\bar{\sigma}_M}\right)\dot{\bar{\sigma}}_A \tag{2}$$

The consistency condition for the active yield surface $\mathbf{\Phi}_A$ as a function of σ_{ij}, α_{ij}^A and $\bar{\sigma}_A$ during the unloading/reloading process can be expressed as

$$\dot{\Phi}_A\left(\sigma_{ij},\alpha_{ij}^{A},\bar{\sigma}_A\right)=\frac{\partial\Phi_A}{\partial\sigma_{ij}}\dot{\sigma}_{ij}+\frac{\partial\Phi_A}{\partial\alpha_{ij}^{A}}\dot{\alpha}_{ij}^{A}+\frac{\partial\Phi_A}{\partial\bar{\sigma}_A}\dot{\bar{\sigma}}_A=0 \tag{3}$$

where $\bar{\sigma}_A$ is not a constant but increases during the unloading/reloading process. Substituting Eq. (2) into Eq. (3) gives the size increase rate $\dot{\bar{\sigma}}_A$ of the active yield surface. Then, substituting $\dot{\bar{\sigma}}_A$ into Eq. (2) gives the evolution equation for α_{ij}^A of the active yield surface $\mathbf{\Phi}_A$.

Drucker and Prager [6] proposed a phenomenological yield function for pressure-sensitive materials. For the unloading/reloading process, the Drucker-Prager yield function can be expressed with respect to the center of the active yield surface at α_{ij}^{A} as

$$\Phi_A\left(\sigma_{ij},\alpha_{ij}^{A},\overline{\sigma}_A\right)=\sigma_{e,A}+\sqrt{3}\mu\sigma_{m,A}-\overline{\sigma}_A=0 \tag{4}$$

where μ is the pressure sensitivity, $\sigma_{e,A}$ is the relative effective stress based on the Mises yield function, $\sigma_{m,A}$ is the relative mean stress, and $\overline{\sigma}_A$ is the generalized effective stress representing the size of the active yield surface. Here, $\sigma_{e,A}$ and $\sigma_{m,A}$ are defined, respectively, as

$$\sigma_{e,A}=\left[\frac{3}{2}\left(\sigma'_{ij}-\alpha'^{A}_{ij}\right)\left(\sigma'_{ij}-\alpha'^{A}_{ij}\right)\right]^{\frac{1}{2}} \tag{5a}$$

$$\sigma_{m,A}=\frac{\sigma_{kk}-\alpha_{kk}^{A}}{3} \tag{5b}$$

where σ'_{ij} is the deviatoric stress tensor and α'^{A}_{ij} is the deviatoric part of the yield surface center.

A NON-ASSOCIATED FLOW RULE AND CONSTITUTIVE RELATION

A non-associated flow rule based on the Drucker-Prager yield function is adopted here in order to characterize the cyclic plastic behavior of cast iron crankshafts during the fillet rolling process. The Mises plastic potential function $\mathbf{\Phi}_{p,A}$ is employed for the non-associated flow rule and it can be expressed as

$$\Phi_{p,A}\left(\sigma_{ij},\alpha_{ij}^{A},\overline{\sigma}_{p,A}\right)=\sigma_{e,A}-\overline{\sigma}_{p,A}=0 \tag{6}$$

where $\sigma_{e,A}$ is defined in Eq. (5a) and $\overline{\sigma}_A$ represents a fictitious generalized effective stress. The plastic potential function in Eq. (6) is assumed to pass through the current stress point and have the same center as that of the active yield surface in Eq. (4). For metals, the pressure sensitivity μ is usually small in the range of a few percents and the plastic dilatancy is one order of magnitude smaller than that predicted by the associated flow rule [8,9]. For cast irons under compression dominant loading conditions due to the fillet rolling process, the volume change due to graphite particles and the void formation are assumed to be small under large hydrostatic compressive stresses as shown in Chien et al. [1] and Choi and Pan [4]. Consequently, plastic deformation is assumed to mainly come from the nearly plastic incompressible iron matrices. Therefore, the Mises plastic potential function $\mathbf{\Phi}_{p,A}$ that leads to plastic incompressibility is adopted here.

Based on the non-associated flow rule, the plastic strain rate $\dot{\varepsilon}_{ij}^{p}$ can be written as [16]

$$\dot{\varepsilon}_{ij}^{p}=\frac{1}{\overline{E}_p}\left(\frac{\partial\Phi_{p,A}}{\partial\sigma_{ij}}\right)\left(\frac{\partial\Phi_{A}}{\partial\sigma_{kl}}\right)\dot{\sigma}_{kl} \tag{7}$$

where $\overline{E}_p$ represents the generalized plastic modulus from a generalized effective stress-strain curve and is considered as a function of the generalized effective stress which represents the size of the active yield surface. In Eq. (7), $\overline{E}_p$ is defined as

$$\overline{E}_p=\frac{\dot{\overline{\sigma}}}{\dot{\overline{\varepsilon}}^{p}} \tag{8}$$

where $\overline{\sigma}$ and $\overline{\varepsilon}^{p}$ represent the generalized effective stress and the generalized effective plastic strain, respectively.

The generalized plastic modulus $\overline{E}_p$ in Eq. (8) can be related to the plastic modulus E_p of a uniaxial tensile or compressive stress-strain curve. Note here that the plastic moduli $\overline{E}_p$ and E_p are functions of $\overline{\sigma}_A$ and the uniaxial compressive stress σ_{11}, respectively(Choi [13]). In this study, a uniaxial compressive stress-strain curve, where σ_{11} is the only nonzero stress component, is considered as a reference stress-strain curve in view of compression dominant cyclic loading conditions during the fillet rolling process. Writing Eq. (7) under uniaxial compressive loading conditions gives

$$\begin{aligned}\dot{\varepsilon}_{11}^{p}&=\frac{1}{\overline{E}_p}\left(\frac{3\sigma'_{11}}{2\sigma_{e,A}}\right)\left(\frac{3\sigma'_{11}}{2\sigma_{e,A}}+\frac{\mu}{\sqrt{3}}\right)\dot{\sigma}_{11}\\&=\frac{1}{\overline{E}_p}\left(\frac{3\sigma'_{11}}{-2\sigma_{11}}\right)\left(\frac{3\sigma'_{11}}{-2\sigma_{11}}+\frac{\mu}{\sqrt{3}}\right)\dot{\sigma}_{11}=\frac{1}{\overline{E}_p}\left(1-\frac{\mu}{\sqrt{3}}\right)\dot{\sigma}_{11}\end{aligned} \tag{9}$$

Note that $\sigma_{e,A}=-\sigma_{11}$ and $\sigma'_{11}=2\sigma_{11}/3$ under uniaxial compressive loading conditions. Since $E_p=\dot{\sigma}_{11}/\dot{\varepsilon}_{11}^{p}$, the relation between $\overline{E}_p$ and E_p is given from Eq. (9) as

$$\overline{E}_p=\left(1-\frac{\mu}{\sqrt{3}}\right)E_p \tag{10}$$

Under uniaxial compressive loading conditions, $\overline{\sigma}_A$ is expressed as

$$\overline{\sigma}_A=-\left(1-\frac{\mu}{\sqrt{3}}\right)\sigma_{11} \tag{11}$$

Therefore, when the plastic modulus E_p is first determined as a function of σ_{11}, the plastic modulus $\overline{E}_p$ can be obtained as a function of $\overline{\sigma}_A$ based on Eqs. (10) and (11). The detailed description of the non-associated flow rule can be found in Choi [13].

The constitutive relations for the Drucker-Prager yield function with the non-associated flow rule are quite similar to those based on the Mises yield function presented in Choi and Pan [4]. Therefore, the details of the constitutive relations for the Drucker-Prager yield function with the non-associated flow rule are not presented here.

FINITE ELEMENT MODEL OF FILLET ROLLING PROCESS

Fig. 2 shows a two-dimensional finite element model used in this study. Fig. 3a shows a magnified finite element mesh near the contact area of interest between the primary roller and the crankshaft fillet. Fig. 3b shows the definitions of the cylindrical coordinates for the crankshaft fillet. The stresses are expressed in terms of the cylindrical coordinates. Note that 0° represents the vertical downward direction. The details of the finite element model and the boundary conditions for roller loading and roller unloading can be found in Choi and Pan [4]. The material properties for the two rollers and the crankshaft used in this study are listed in Table 1 and they are the same as those used in Choi and Pan [4]. Fig. 4 shows three compressive true stress- true plastic strain curves for the two rollers and the crankshaft used in the finite element analysis. The material constants used in the user material subroutine were determined by finding a best fit to the true stress-true plastic strain curve for the crankshaft. The pressure sensitivity μ used here was 0.03. In the finite element analysis, the secondary roller is given a specific vertical displacement in the negative y direction such that the maximum difference of the fillet surface profiles in the y direction before and after the rolling process is 0.17 mm which is the same as that identified in the shadowgraphs in Chien et al. [1].

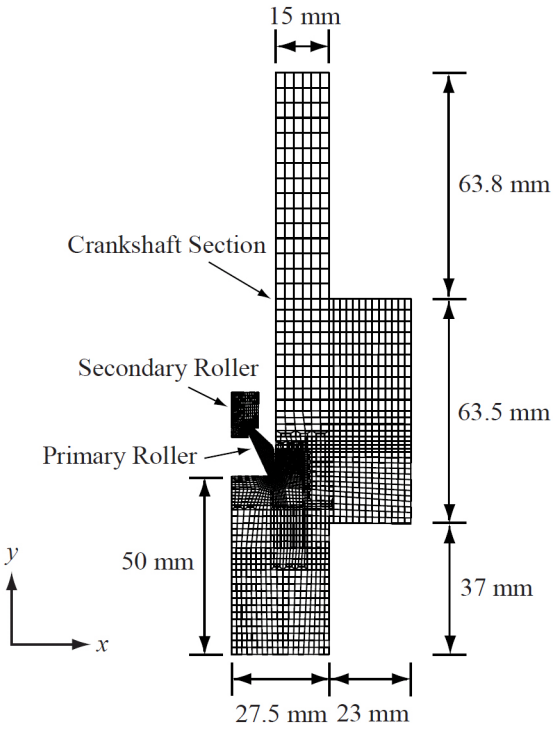

Figure 2. A two-dimensional finite element model consisting of a portion of the crankshaft section, a primary roller and a secondary roller.

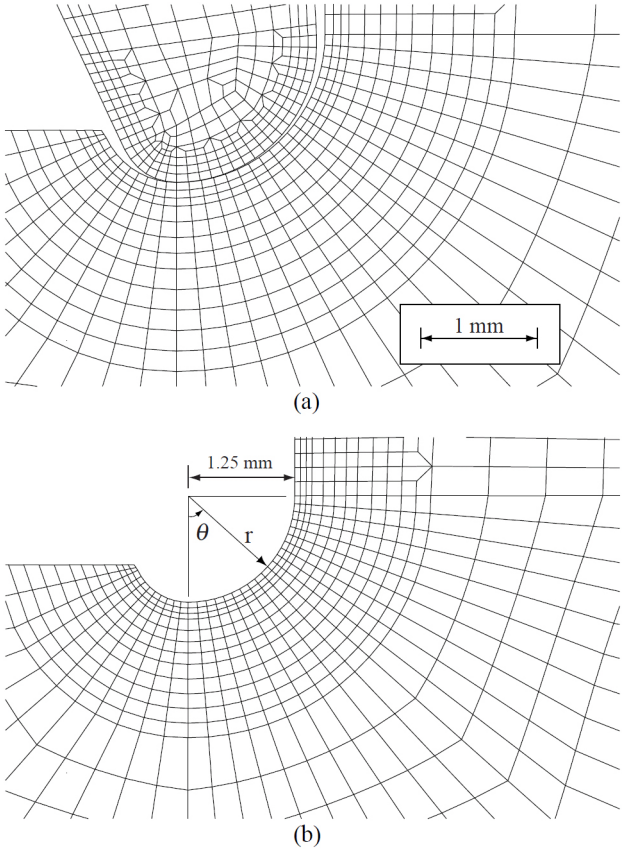

Figure 3. (a) A magnified finite element mesh near the contact area between the primary roller and the crankshaft fillet and (b) the definitions of the cylindrical coordinates for the crankshaft fillet.

Table 1. The material properties for the rollers and the crankshaft used in the finite element analysis.

Material	Primary roller	Secondary roller	Crankshaft
Young's modulus E (GPa)	214	214	169
Poisson's ratio ν	0.29	0.29	0.283
Yield strength σ_y (MPa)	2,338	2,020	462(Compression) 446(Tension)

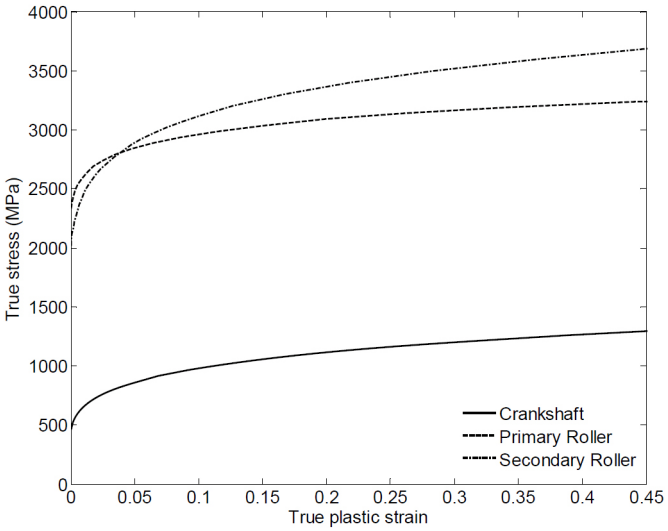

Figure 4. Compressive true stress-true plastic strain curves for the rollers and the crankshaft used in the finite element analysis.

STRESS DISTRIBUTIONS NEAR CRANKSHAFT FILLET

The finite element model shown in Fig. 2 was adopted to investigate the influence of the pressure-sensitive yielding and the non-associated flow rule on the stress distributions near the crankshaft fillet. First, the stress distribution near the fillet based on the associated flow rule with $\mu = 0$ (von Mises) and $\mu = 0.03$ (Drucker-Prager), and the non-associated flow rule with $\mu = 0.03$ (Drucker-Prager) are shown in Fig. 5 when the roller is down. Fig. 5a shows the radial distributions of the stresses at $\theta = 42°$ as functions of the distance from the fillet surface. It should be noted that the bending stresses are typically large near 40° to 45° [1] and cracks usually were initiated near that region. Therefore, the angle $\theta = 42°$ is selected for the demonstration purpose. Fig. 5b shows the angular distributions of the stresses along the fillet surface as functions of θ from 0° to 90°. Here, for the associated flow rule with $\mu = 0$ and $\mu = 0.03$, and the non-associated flow rule with $\mu = 0.03$, the secondary rollers are given the displacements of 0.468 mm, 0.4885 mm, and 0.4795 mm, respectively, in the negative y direction to induce the maximum difference of the fillet surface profiles of 0.17 mm.

As shown in the figures, the stress distributions for $\mu = 0$ and $\mu = 0.03$ based on the two flow rules show almost the same trends both along the fillet surface and in the radial direction only with small differences in their magnitudes. Note that, even with the same uniaxial compressive stress-strain curve, the pressure-sensitive materials under compression show different behaviors for different μ's and different flow rules under plane strain loading conditions, due to the constraint in the out-of-plane direction.

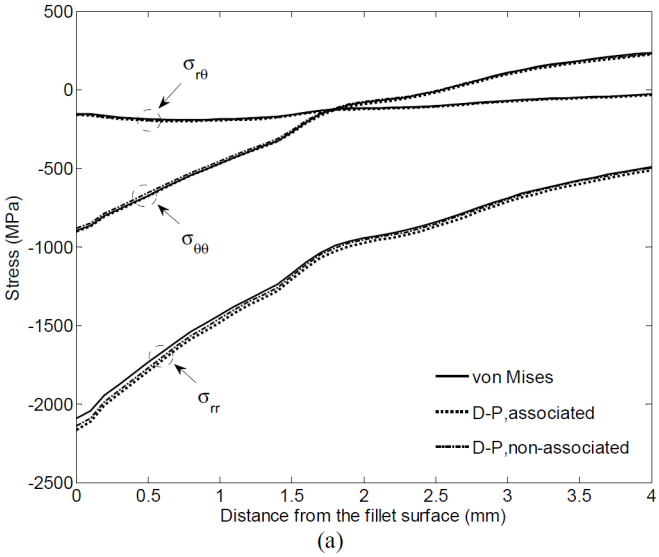

Figure 5.

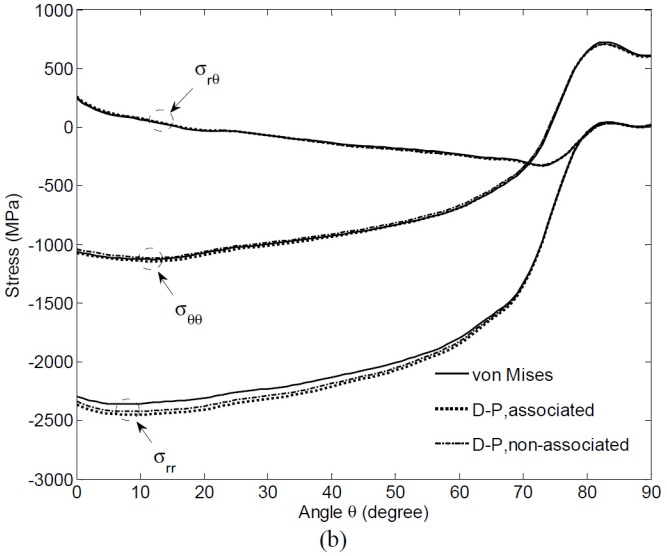

Figure 5. (cont.) The distributions of the hoop stress $\sigma_{\theta\theta}$, the radial stress σ_{rr}, and the shear stress $\sigma_{r\theta}$ based on the von Mises yield function and the Drucker-Prager yield function with $\mu = 0.03$ and different flow rules when the roller is down. (a) The radial distributions of the stresses at $\theta = 42°$ and (b) the angular distributions of the stresses along the fillet surface.

When the roller is released, the distributions of the residual hoop stress $\sigma_{\theta\theta}$, the residual radial stress σ_{rr}, and the residual shear stress $\sigma_{r\theta}$ near the fillet for $\mu = 0$ and $\mu = 0.03$ with the associated and non-associated flow rules are shown in Fig. 6. Since the residual hoop stress $\sigma_{\theta\theta}$ near the fillet surface is important in the crankshaft section to determine the fatigue failure behaviors, we should pay attention to the distributions of the residual hoop stress $\sigma_{\theta\theta}$ near the fillet surface. Fig. 6a shows the radial distributions of the stresses at $\theta = 42°$ as functions of the distance from the fillet surface. As shown in Fig. 6a, within the depth of about 2 mm from the fillet surface, the magnitude of the compressive residual hoop stress $\sigma_{\theta\theta}$ decreases as μ increases. As for the two different flow rules, the stress distributions for $\mu = 0.03$ show the same trends in the radial direction, but the magnitude of the compressive residual hoop stress $\sigma_{\theta\theta}$ based on the non-associated flow rule is smaller than that based on the associated flow rule. Note that the compressive residual hoop stress $\sigma_{\theta\theta}$ within the depth of 2 mm show relatively large different magnitudes for $\mu = 0$ based on the associated flow rule and $\mu = 0.03$ based on the non-associated flow rule.

Fig. 6b shows the angular distributions of the stresses along the fillet surface as functions of θ from 0° to 90°. As shown in Fig. 6b, the distributions of the compressive residual hoop stress $\sigma_{\theta\theta}$ along the fillet surface based on the associated flow rule with $\mu = 0$ and $\mu = 0.03$, and the non-associated flow rule with $\mu = 0.03$ show the similar trends along the fillet surface. The magnitude of the compressive residual hoop stress $\sigma_{\theta\theta}$ along the fillet surface generally decreases as μ increases except for the region with the angle larger than $\theta = 80°$. Besides, the magnitude of the compressive residual hoop stress $\sigma_{\theta\theta}$ for $\mu = 0.03$ based on the non-associated flow rule is smaller than that based on the associated flow rule along the fillet surface. The compressive residual hoop stress $\sigma_{\theta\theta}$ along the fillet surface also show relatively large different magnitudes for $\mu = 0$ based on the associated flow rule and $\mu = 0.03$ with the non-associated flow rule.

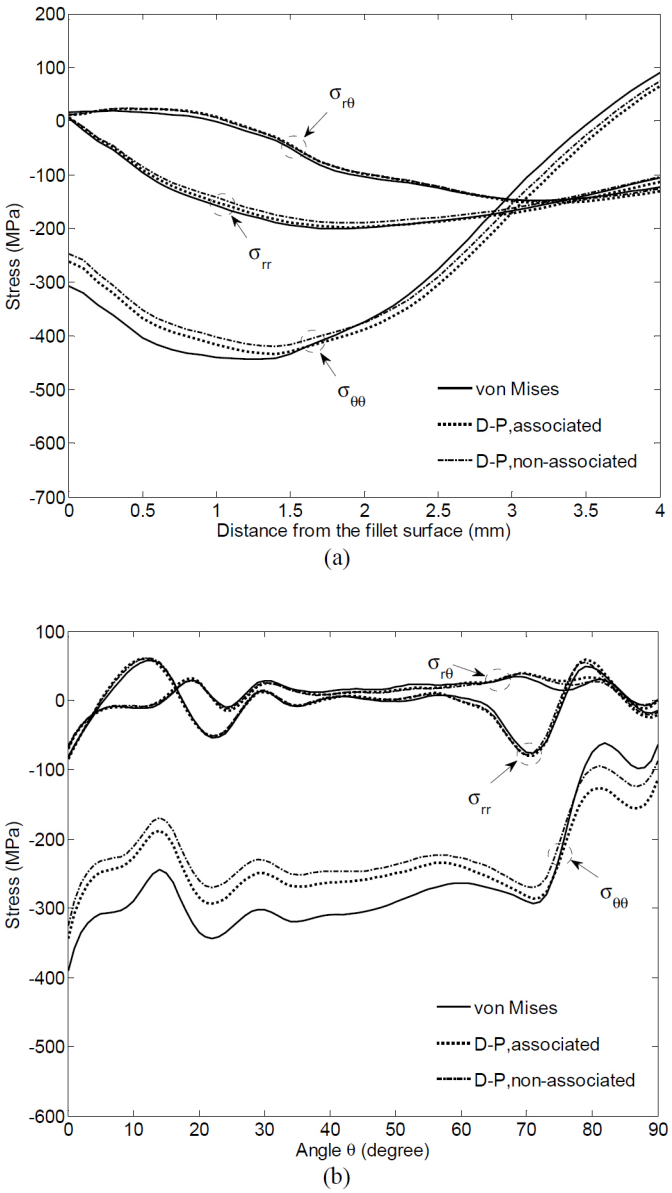

Figure 6. The distributions of the residual hoop stress $\sigma_{\theta\theta}$, the residual radial stress σ_{rr}, and the residual shear stress $\sigma_{r\theta}$ based on the von Mises yield function and the Drucker-Prager yield function with $\mu = 0.03$ and different flow rules when the roller is released. (a) The radial distributions of the stresses at $\theta = 42°$ and (b) the angular distributions of the stresses along the fillet surface.

SUMMARY/CONCLUSIONS

In this paper, the non-associated flow rule proposed by Choi [13] for pressure-sensitive materials under cyclic loading conditions is employed in a two-dimensional finite element analysis of a crankshaft section under fillet rolling. The evolution equation for the active yield surface during the unloading/reloading process is first presented based on the anisotropic hardening rule of Choi [13]. Here, the pressure-sensitive Drucker-Prager yield function is adopted for cast iron crankshafts to characterize the pressure-sensitive plastic behavior of cast irons due to the different stress-strain curves under tension and compression. A user material subroutine based on the anisotropic hardening rule and the constitutive relation was written and implemented into the commercial finite element program ABAQUS.

A two-dimensional plane-strain finite element analysis of a crankshaft section under fillet rolling was conducted for different values of the pressure sensitivity and different flow rules in order to investigate the effect of the pressure-sensitive yielding and the non-associated flow rule on the stress distributions near the fillet. For the magnitude of the residual hoop stress which is the important stress component in the crankshaft section to determine the fatigue failure behaviors, the magnitude of the compressive residual hoop stress decreases as the pressure sensitivity increases within the depth of 2 mm from the fillet surface. In addition, the magnitude of the compressive residual hoop stress for pressure-sensitive materials with the non-associated flow rule is smaller than that with the associated flow rule. Since the pressure sensitivity and the non-associated flow rule have noticeable influence on the magnitude of the residual stresses near the fillet surface, the effect of pressure sensitivity and the non-associated flow rule need to be considered in simulations of cast iron crankshafts under fillet rolling.

REFERENCES

1. Chien, W.Y., Pan, J., Close, D., and Ho, S., "Fatigue Analysis of Crankshaft Sections under Bending with Consideration of Residual Stresses," *International Journal of Fatigue* 27(1):1-19, 2005, doi:10.1016/j.ijfatigue.2004.06.009.
2. Spiteri, P., Lee, Y., and Segar, R., "An Exploration of Failure Modes in Rolled, Ductile, Cast-Iron Crankshafts Using a Resonant Bending Testing Rig," SAE Technical Paper 2005-01-1906, 2005, doi:10.4271/2005-01-1906.
3. Spiteri, P., Ho, S., and Lee, Y.-L., "Assessment of Bending Fatigue Limit for Crankshaft Sections with Inclusion of Residual Stresses," *International Journal of Fatigue* 29(2):318-329, 2007, doi:10.1016/j.ijfatigue.2006.03.009.
4. Choi, K.S. and Pan, J., "Simulations of Stress Distributions in Crankshaft Sections under Fillet Rolling and Bending Fatigue Tests," *International Journal of Fatigue* 31(3):544-557, 2009, doi:10.1016/j.ijfatigue.2008.03.035.
5. Choi, K.S. and Pan, J., "Effects of Pressure-Sensitive Yielding on Stress Distributions in Crankshaft Sections under Fillet Rolling and Bending Fatigue Tests," *International Journal of Fatigue* 31(10):1588-1597, 2009, doi:10.1016/j.ijfatigue.2009.04.007.
6. Drucker, D.C. and Prager, W., "Soil Mechanics and Plastic Analysis or Limit Design," *Quarterly of Applied Mathematics* 10(2):157-165, 1952.
7. Spitzig, W.A. and Richmond, O., "Effect of Hydrostatic Pressure on the Deformation Behavior of Polyethylene and Polycarbonate in Tension and in Compression," *Polymer Engineering & Science* 19(16):1129-1139, 1979, doi:10.1002/pen.760191602.
8. Spitzig, W.A. and Richmond, O., "The Effect of Pressure on the Flow Stress of Metals," *Acta Metallurgica* 32(3):457-463, 1984, doi:10.1016/0001-6160(84)90119-6.
9. Richmond, O. and Spitzig, W.A., "Pressure Dependence and Dilatancy of Plastic Flow," Proceedings of 15th International Congress of Theoretical and Applied Mechanics, North-Holland Publishing Co., Amsterdam, Toronto, Canada: 377-386, 1980.
10. Brünig, M., "Numerical Simulation of the Large Elastic-Plastic Deformation Behavior of Hydrostatic Stress-Sensitive Solids," *International Journal of Plasticity* 15(11):1237-1264, 1999, doi:10.1016/S0749-6419(99)00042-X.
11. Altenbach, H., Stoychev, G.B., and Tushtev, K.N., "On Elastoplastic Deformation of Grey Cast Iron," *International Journal of Plasticity* 17(5):719-736, 2001, doi:10.1016/S0749-6419(00)00026-7.
12. Stoughton, T.B. and Yoon, J.-W., "A Pressure-Sensitive Yield Criterion under a Non-Associated Flow Rule for Sheet Metal Forming," *International Journal of Plasticity* 20(4-5):705-731, 2004, doi:10.1016/S0749-6419(03)00079-2.

13. Choi, K.S., "Residual Stress near Fillet and Roller Fatigue in Crankshaft Fillet Rolling Process," Ph.D. Thesis, University of Michigan, Ann Arbor, Michigan, 2007.
14. Mróz, Z., "On the Description of Anisotropic Workhardening," *Journal of the Mechanics and Physics of Solids* 15(3):163-175, 1967, doi:10.1016/0022-5096(67)90030-0.
15. Mróz, Z., "An Attempt to Describe the Behavior of Metals under Cyclic Loads Using a More General Workhardening Model," *Acta Mechanica* 7(2-3):199-212, 1969, doi:10.1007/BF01176668.
16. Rice, J.R., "The Localization of Plastic Deformation," Proceedings of 14th International Congress of Theoretical and Applied Mechanics, North-Holland Publishing Co., Amsterdam, Delft, The Netherlands: 207-220, 1976.

CONTACT INFORMATION

Professor Jwo Pan
Mechanical Engineering
The University of Michigan
Ann Arbor, MI 48109-2125
Telephone: 734-764-9404
Fax: 734-647-3170
jwo@umich.edu

ACKNOWLEDGMENTS

The support of this work by the Ford-University of Michigan Alliance Program is greatly appreciated.